

MOTGNN: Interpretable Graph Neural Networks for Multi-Omics Disease Classification

Tiantian Yang

University of Idaho
Moscow, Idaho, USA
tyang@uidaho.edu

Zhiqian Chen

Mississippi State University
Starkville, Mississippi, USA
zchen@cse.msstate.edu

Abstract

Integrating multi-omics data, such as DNA methylation, mRNA expression, and microRNA (miRNA) expression, offers a comprehensive view of the biological mechanisms underlying disease. However, the high dimensionality and complex interactions among omics layers present major challenges for predictive modeling. We propose Multi-Omics integration with Tree-generated Graph Neural Network (**MOTGNN**), a novel and interpretable framework for binary disease classification. MOTGNN employs eXtreme Gradient Boosting (XGBoost) to perform omics-specific supervised graph construction, followed by modality-specific Graph Neural Networks (GNNs) for hierarchical representation learning, and a deep feedforward network for cross-omics integration. On three real-world disease datasets, MOTGNN outperforms state-of-the-art baselines by 5-10% in accuracy, ROC-AUC, and F1-score, and remains robust to severe class imbalance (e.g., 87.2% vs. 33.4% F1 on imbalanced data). The model maintains computational efficiency through sparse graphs (2.1-2.8 edges per node) and provides built-in interpretability, revealing both top-ranked biomarkers and the relative contributions of each omics modality. These results highlight MOTGNN's potential to improve both predictive accuracy and interpretability in multi-omics disease modeling.

Keywords

Graph neural networks, Multi-omics integration, XGBoost, Disease classification, Model interpretability

1 Introduction

A comprehensive understanding of complex diseases, such as cancer, cardiovascular disease, and neurodegenerative disorders, is critical for advancing public health and enabling precision medicine. These diseases are not driven by isolated molecular events but emerge from intricate interactions among genomic, epigenomic, and transcriptomic factors [32]. Recent advances in high-throughput biotechnologies have enabled the simultaneous collection of different layers of molecular regulation, such as gene expression (messenger RNA), epigenetic modifications (DNA methylation), and non-coding RNA activity (e.g., microRNA), from the same set of biological samples [14]. These omics datasets capture intricate relationships among biological entities and molecular processes, offering insights into disease mechanisms. While individual omics types provide valuable information, different modalities reflect distinct biological processes and contribute complementary information. Integrating multiple omics (multi-omics) data is essential to comprehensively understand the complex, multi-layered systems underlying disease processes and their progression [36]. However, integrating heterogeneous omics data presents unique challenges.

A fundamental issue is that the number of samples (n) is substantially smaller than the number of features (p). For example, a study may involve only a few hundred participants while measuring tens of thousands of molecular features. This high dimensionality complicates learning and increases the risk of overfitting. Moreover, not all measured features are biologically relevant; noisy or redundant features can obscure meaningful patterns. Although prior biological knowledge, such as gene-gene or protein-protein interactions, has been identified experimentally, our knowledge is constrained by experimental design and equipment constraints. Consequently, there is a growing need for computational models that can reliably infer biologically meaningful structures and interactions from multi-omics data [17].

Traditional machine learning and deep learning models have been extensively applied to address the high dimensionality and complexity of omics data [2, 44], but most of these approaches assume a Euclidean data structure. Classical machine learning methods, such as random forests [4] and gradient boosting methods, such as XGBoost [6], operate by constructing ensembles of decision trees and are effective for classification tasks, but they typically treat features as independent and fail to capture structural relationships among them. Deep learning models [24], such as deep feedforward networks (DFNs) [11], convolutional neural networks, and recurrent neural networks, can model nonlinear feature dependencies but are not designed to process non-Euclidean data structures such as graphs. These approaches typically require large training sets to avoid overfitting. Moreover, their black-box nature often limits interpretability, which is essential in biomedical applications where transparency and reproducibility are critical. Furthermore, concatenating features from different omics modalities as input can obscure modality-specific relationships and introduce additional noise. Graph-based approaches offer a natural alternative for modeling complex biological systems. In omics applications, nodes can represent features (e.g., genes) or samples, and edges encode various relationships, such as similarity, co-expression, or learned interactions. Graph Neural Networks (GNNs) [5, 7, 39, 46, 50] have emerged as powerful tools for learning from graph-structured data by recursively aggregating information from each node's neighborhood. GNNs capture both local and global graph topology and have found increasing use in biomedical applications, including molecular modeling, medical imaging, drug discovery, and disease prediction [18, 36, 45, 49]. Foundational models such as message passing neural networks (MPNNs) [10], graph convolutional networks (GCNs) [21], graph attention networks (GATs) [31], GraphSAGE [13], and graph isomorphism networks (GINs) [40] have significantly advanced the expressiveness and scalability of GNN-based learning.

Despite recent advances, applying GNNs to multi-omics data remains challenging and relatively underexplored [3, 30, 34, 45]. The irregular nature of graph-structured data further complicates this task, as each node may have a variable number of neighbors, and many standard deep learning operations are not directly applicable in this setting [7]. Although several GNN-based frameworks have been proposed for multi-omics integration, many of these works exhibit substantial limitations, which we summarize into three main areas: (1) **Inadequate modeling of high-dimensional, heterogeneous omics data**: To address high dimensionality (i.e., the “small n , large p ” issue), existing methods typically apply simple filtering techniques, such as removing low-variance or zero-valued features, or selecting features based on univariate statistical tests. Some approaches flatten multi-omics data by concatenating omics layers before graph construction, which weakens modality-specific signals and ignores biological heterogeneity. Others rely heavily on hand-crafted similarity graphs (e.g., Pearson or cosine similarity), which may miss nonlinear, task-specific relationships, ignore the sparse and scale-free nature of biological graphs, and are sensitive to arbitrary thresholding or preprocessing pipelines. (2) **Vulnerability to class imbalance**: While class imbalance is prevalent in biomedical datasets (e.g., rare diseases, early-stage cancer detections, or minority subtypes), it is rarely addressed during model development or evaluation. Many existing models optimize for overall accuracy, which can be misleading when predictions favor the majority class. In these scenarios, even high accuracy may reflect poor minority class detection. As a result, these approaches often lack robustness and generalizability in imbalanced settings, where accurate prediction of minority cases is of greater biological and clinical importance. (3) **Limited interpretability and biological insight**: Interpretability is essential in biomedical research, as understanding which features or omics modalities drive predictions is essential for trust, transparency, and downstream biological discovery. However, most existing GNN-based models lack built-in interpretability. Instead, they rely on computationally intensive post hoc analyses or ablation studies to infer importance, which are not scalable and may introduce instability. In addition, they typically treat all omics types equally, failing to uncover their relative contributions. To address these limitations, we propose MOTGNN, a novel and interpretable graph-based framework for multi-omics data integration that combines supervised graph construction with hierarchical representation learning. Our key contributions are as follows:

- **Modality-specific modeling with supervised graph learning**: We utilize XGBoost to filter informative features for each omics type, and leverage the structure of the trained decision trees to construct sparse, supervised, and modality-specific graphs. This approach preserves biologically meaningful interactions while reducing noise and redundancy. We then apply GNNs to learn latent representations from each graph, which are integrated through a DFN to model cross-omics interactions.
- **Imbalance-robust architecture**: MOTGNN consistently outperforms existing models across all datasets, achieving 10–50% improvement in F1-score on class-imbalanced real-world data. Its design mitigates overfitting to the dominant classes

and remains effective in detecting minority class signals, addressing a critical limitation in biomedical classification tasks.

- **Integrated interpretability at feature and omics levels**: MOTGNN enables end-to-end interpretability without requiring post hoc analysis. It provides (i) feature-level importance scores to identify top-ranked biomarkers within each modality, and (ii) omics-level contribution scores, offering insights into which data types (e.g., methylation, mRNA, or miRNA) are most influential for prediction. This layered interpretability potentially supports downstream biological discovery and facilitates clinical relevance.

2 Related Work

Many advanced deep learning methods have been developed by incorporating novel model components to analyze omics data. For example, MOCAT [42] leverages an autoencoder, three omics-specific classifiers, a multi-head attention mechanism, and a confidence network (ConfNet) to integrate and learn from multi-omics data (e.g., methylation, mRNA, and miRNA). However, it lacks the ability to capture topological information and thus may miss important structural insights. Some GNN-based methods have been developed for single-omics data analysis in disease classification or cancer subtype prediction. For example, forgenet [23] constructs a supervised directed graph using a tree-ensemble model, but it uses the original high-dimensional data without dimension reduction, leading to high computational costs. Moreover, it only uses a single omics type, which provides limited information compared to multi-omics integration. DMGCN [41] integrates multiple biological networks via GCNs, but also focuses on a single omics modality and does not utilize cross-omics information.

More recent GNN-based methods aim to integrate multi-omics data for disease classification, cancer subtype analysis, and survival prediction. MOGONET [35] proposes a GCN-based framework to integrate multi-omics data (methylation, mRNA, and miRNA), using a cross-omics discovery tensor and a view correlation discovery network for final label prediction. However, it identifies important features through computationally expensive ablation studies. In addition, its graph construction is based on cosine similarity with a manually selected threshold determined by a hyperparameter (edge-to-node ratio), which must be tuned. MODILM [48] shares a similar architecture with MOGONET but uses GAT instead of GCN. CLCLSA [47] handles incomplete multi-omics classification using cross-omics autoencoders to recover missing omics representations, contrastive learning to align representations, and self-attention at both the feature and omics levels for feature selection, but does not explicitly leverage graph structures. SUPREME [19] employs GCNs and patient similarity networks, integrating seven types of omics data for cancer subtype prediction and survival analysis. However, it also relies on ablation studies to determine the most effective omics combinations. MOGAT [33] focuses on survival analysis with a similar structure to SUPREME, but uses GAT instead of GCN. It conducted integration studies with two to eight omics types and found that using three omics achieved the best performance for breast cancer subtype prediction, suggesting that

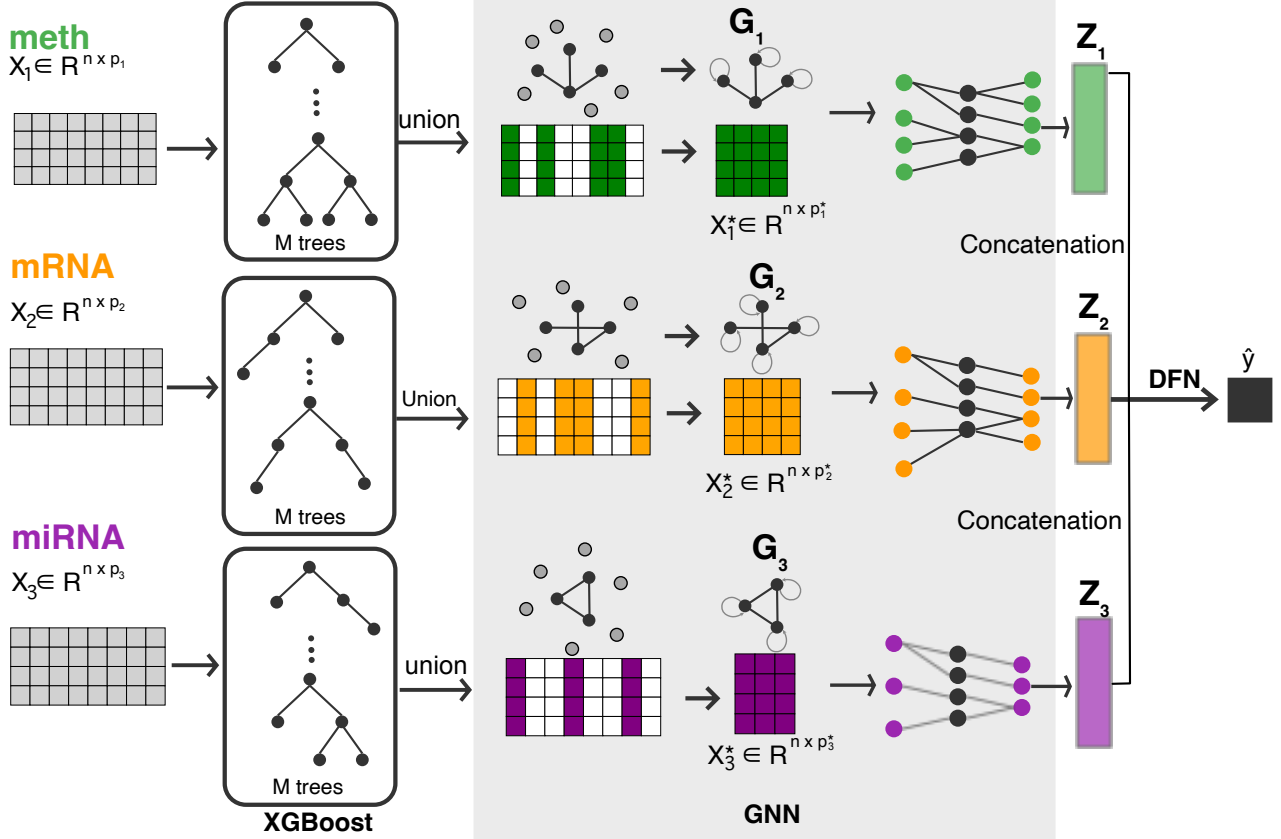


Figure 1: Overview of the proposed MOTGNN framework, which involves three key modules: (i) XGBoost for graph construction within each omics modality; (ii) GNN for learning modality-specific embeddings by encoding both feature graphs and associated data matrices; and (iii) DFN that integrates the learned embeddings and performs classification.

adding more omics data does not always yield better results. However, MOGAT does not address model interpretability, as it does not identify important biomarkers. DeepMoIC [38] integrates three types of omics data to address cancer subtype classification by combining autoencoders, similarity network fusion, and a deep GCN with residual connections and identity mappings. However, it constructs patient similarity networks to guide the learning and lacks omics-wise interpretability. MoGCN [25] targets breast cancer subtype classification using multi-omics data (copy number variation, RPPA, and RNA-seq). It applies autoencoders for dimensionality reduction and similarity network fusion for graph construction, and trains a GCN model on the resulting fused network. However, its graph construction still relies on distance-based methods.

While these models demonstrate promising results, several common limitations remain: They require extensive data preprocessing, and the quality of such preprocessing can significantly affect downstream model performance. Their graph construction approaches rely on simple similarity metrics, which often fail to capture task-relevant nonlinear interactions and can introduce bias due to arbitrary thresholding. They rarely address the class imbalance issue, which is prevalent in biomedical datasets and can significantly impact performance. They commonly depend on ablation studies to

identify the optimal combination of omics data types, a computationally expensive process that is not easily scalable.

3 Methodology

We summarized the key notations and their associated descriptions in Table 1. A graph is denoted as $G(V, E)$, where V represents the set of vertices (or nodes) and E denotes the set of edges. Graph structure is encoded by its adjacency matrix A , in which the (i, j) -th element is one if node i is connected to node j , and zero otherwise. For undirected graphs, A is symmetric. The adjacency matrix augmented with self-loops is denoted as \tilde{A} , where all diagonal elements are set to one to include self-connections.

3.1 Proposed Model

We propose a Multi-Omics integration framework with Tree-generated Graph Neural Network (MOTGNN) model for binary disease classification. MOTGNN first leverages eXtreme Gradient Boosting (XGBoost) to select informative features in a supervised manner, as the tree-based feature selection captures strong predictive signals. It then utilizes GNNs to learn omics-specific representations from graphs constructed using the structure of trained XGBoost

Table 1: Key notations and descriptions

Notation	Description
G or $G(V, E)$	Graph
V	Set of vertices/nodes in G
E	Set of edges in G
A	Adjacency matrix of G
\tilde{A}	Adjacency matrix with self-loops
$X_i \in \mathbb{R}^{n \times p_i}$	Omics data matrix for modality $i = 1, 2, 3$
n	Number of samples (rows in X_i)
p_i	Number of features in X_i
Y	Binary outcome variable
$X_i^* \in \mathbb{R}^{n \times p_i^*}$	Dimension-reduced representation of X_i
p_i^*	Reduced feature dimension for X_i
G_i or $G_i(V_i, E_i)$	Graph constructed for X_i^*
V_i	Set of vertices/nodes in G_i
E_i	Set of edges in G_i
Z_i	Embedding learned from G_i via GNN
Z	Concatenated representation of all Z_i
m_i	Edge-to-node ratio, i.e., $m_i = \frac{ E_i }{p_i^*}$
RIG_i	Relative importance of graph G_i
\odot	Element-wise (Hadamard) product
$I(\cdot)$	Indicator function

trees. This combination allows the model to extract both local and global patterns from each omics layer while maintaining biological interpretability.

The framework of MOTGNN is shown in Figure 1, which consists of three primary modules: (1) An **XGBoost module** for feature graph construction; (2) A **GNN module** to encode each omics-specific graph and its associated data matrix; and (3) A **DFN module** to integrate and classify the learned embeddings. This modular architecture allows MOTGNN to handle high-dimensional, heterogeneous multi-omics data efficiently while providing interpretable insights at both the feature and omics-layer levels. Algorithm 1 demonstrates the steps of the overall structure of MOTGNN.

Algorithm 1 MOTGNN

Require: Omics datasets: $X_1 \in \mathbb{R}^{n \times p_1}$, $X_2 \in \mathbb{R}^{n \times p_2}$, $X_3 \in \mathbb{R}^{n \times p_3}$; Binary disease labels: $Y \in \mathbb{R}^{n \times 1}$
Ensure: Predicted labels \hat{Y}

- 1: Train three XGBoost models using X_1 , X_2 , and X_3 to predict Y
- 2: Construct omic-specific feature graphs: $G_1(V_1, E_1)$, $G_2(V_2, E_2)$, and $G_3(V_3, E_3)$ by taking the union of decision paths from all trees trained in Step 1, along with the corresponding dimension-reduced datasets: $X_1^* \in \mathbb{R}^{n \times p_1^*}$, $X_2^* \in \mathbb{R}^{n \times p_2^*}$, and $X_3^* \in \mathbb{R}^{n \times p_3^*}$
- 3: **for** each (X_i^*, G_i) , $i = 1, 2, 3$ **do**
- 4: Feed X_i^* and \tilde{A}_i (augmented adjacency matrix of G_i with self-loops) into a GNN
- 5: Obtain learned embedding Z_i
- 6: **end for**
- 7: Concatenate Z_1 , Z_2 , and Z_3 to form a unified representation
- 8: Pass the concatenated representation Z into a DFN to perform final binary classification
- 9: **return** Predicted classification labels \hat{Y}

3.2 Graph Construction

XGBoost [6] is a powerful ensemble method based on gradient-boosted decision trees. Compared to traditional gradient boosting machines (GBMs) [9], XGBoost introduces a regularized learning objective to reduce overfitting and improve generalization. In MOTGNN, we employ three XGBoost models, each trained independently to perform binary classification on the omics-specific datasets X_1 , X_2 , and X_3 alongside the binary response Y . Unlike random forest, which generates independent trees, each trained XGBoost model generates M sequential decision trees, where every tree improves upon the residuals of the previous ones. During training, each tree selects a subset of features for node splits. We collect the union of all features used across the M trees and define these as the selected features. This yields a supervised, tree-guided feature selection process that reduces the original feature dimensions from p_1 , p_2 , and p_3 to p_1^* , p_2^* , and p_3^* , respectively, where $p_i^* < p_i$ and $p_1^* \neq p_2^* \neq p_3^*$. The reduced dimensions preserve features with higher predictive importance, facilitating downstream graph construction and neural modeling.

Inspired by forgeNet [23], which constructs feature graphs based on the structure of ensemble trees, we adapt this approach to build omics-specific undirected graphs from XGBoost models. Specifically, for each omics dataset, we treat each trained decision tree as a graph, where features involved in splits are nodes, and parent-child relationships form the undirected edges. Taking $X_1 \in \mathbb{R}^{n \times p_1}$ along with the binary outcome Y as an example, suppose the XGBoost model generates M sequential decision trees. Each tree is considered an undirected graph $G^m = (V^m, E^m)$ for $m = 1, 2, \dots, M$. We then take the union of all tree-level graphs to form the aggregated graph $G_1 = (V_1, E_1)$ as:

$$G_1(V_1, E_1) = G_1\left(\bigcup_{m=1}^M V^m, \bigcup_{m=1}^M E^m\right),$$

where the number of nodes in G_1 is $|V_1| = p_1^*$, and $p_1^* < p_1$. We also add self-loops to the adjacency matrices to preserve self-information in GNN message passing. A similar procedure generates G_2 and G_3 for the remaining two omics datasets.

3.3 Graph Neural Network and Feature Fusion

We utilize the graph-embedded deep feedforward network (GEDFN) model [22] as the core GNN component used in MOTGNN. Unlike standard fully connected architectures, GEDFN directly incorporates the adjacency matrix into the weight connections between the input and the first hidden layers. This design enables the model to respect the feature-level relationships encoded in the graph while enforcing the sparsity, a common assumption for omics-based feature graphs. The number of neurons in the first hidden layer must be the same as the input dimension. Formally, given the reduced input data $X^* \in \mathbb{R}^{n \times p^*}$ and its graph adjacency matrix $\tilde{A} \in \mathbb{R}^{p^* \times p^*}$ (augmented with self-loops), the first hidden layer $Z_1 \in \mathbb{R}^{n \times p^*}$ is computed as

$$Z_1 = \sigma(X^*(W_{in} \odot \tilde{A}) + b_{in}),$$

where $W_{in} \in \mathbb{R}^{p^* \times p^*}$ and $b_{in} \in \mathbb{R}^{n \times p^*}$ are the weight and bias matrices, \odot denotes element-wise (Hadamard) multiplication, and $\sigma(\cdot)$ is the activation function. The design of GEDFN shares conceptual

similarities with the graph attention network (GAT) formulation discussed in [7], where the GAT layer is represented as

$$Z_1 = \sigma((W_{\text{attention}} \odot A)X + b_{in}),$$

with $W_{\text{attention}} \in \mathbb{R}^{n \times n}$ and the nodes representing samples rather than features. In this formulation, GAT dynamically learns attention weights over neighbors. Similarly, GEDFN enables dynamic weight learning while ensuring that connections between features and the first hidden layer are strictly supported by the feature graph. This yields a sparse and interpretable architecture tailored to omics data.

Following the training of three omics-specific GNNs, each on its respective dimension-reduced input and constructed graph, we obtain three last hidden representations: Z_1 , Z_2 , and Z_3 . These embeddings are concatenated to form a unified representation:

$$Z = [Z_1 | Z_2 | Z_3],$$

where Z denotes the concatenated neurons, and is then passed to a DFN, which consists of fully connected layers and a final softmax output to perform binary disease classification.

3.4 Interpretability on Features and Graphs

To interpret model predictions and evaluate the contribution of features and graphs, we adopt and extend the connection weights method [29]. Feature importance is assessed by summing the absolute weights connecting each input neuron to the first hidden layer, while accounting for adjacency-based sparsity. For feature j in X_i , the importance score IF_j^i is defined as:

$$IF_j^i = \sum_{u=1}^{p_i} \left| W_{ju}^{(in)} I(\tilde{A}_{ju}^i = 1) \right|,$$

where $W^{(\text{in})}$ is the input weight matrix and $I(\cdot)$ is the indicator function. After training the model, each input feature is assigned an importance score. These scores can be used to rank the features, allowing the selection of top biomarkers for further biological investigation. To evaluate the relative importance of the graph for each omics modality, we compute the L_1 norm of the weight matrix connecting the GNN's last hidden representations (Z_i) to the DFN layer. The relative graph importance (RIG) is then:

$$RIG_i = \frac{\|W_{Z_i \leftrightarrow f}\|_1}{\sum_{i=1}^3 \|W_{Z_i \leftrightarrow f}\|_1},$$

where $i = 1, 2, 3$, $W_{Z_i \leftrightarrow f}$ is the weight matrix connecting Z_i and DFN, and $\|\cdot\|_1$ is the L_1 norm that sums the absolute values of its inside matrix. The total contribution sums to one across all three graphs.

3.5 Technical Details

We implement the xgboost Python library [6] for the XGBoost module in MOTGNN. We tuned the number of estimators (determine trees). We employ the Tensorflow library [1] for training GNN and DFN modules. Model optimization uses the Adam optimizer [20] with mini-batch training. The nonlinear activation function uses the Rectified Linear Unit (ReLU) function: $\sigma(x) = \max(0, x)$ [28]. For classification, the final output layer uses a softmax function,

and the loss is computed using binary cross-entropy:

$$L(Y, \hat{Y}) = -\frac{1}{n} \sum_{i=1}^n \{y_i \ln(\hat{y}_i) + (1 - y_i) \ln(1 - \hat{y}_i)\}.$$

We tune hyperparameters across three main categories: (1) architectural (number of layers and hidden neurons), (2) training-related (learning rate, batch size, and epochs), and (3) regularization-related (dropout and L2 penalty). To avoid overfitting, we apply strategies including dropout, batch normalization, L2 regularization, and early stopping. Data are split into training, validation, and test sets in a 60%:20%:20% ratio, with stratified sampling to address class imbalance. We have conducted 20 independent and reproducible train-validation-test splits. Hyperparameters are tuned via grid search in a reasonable space and based on experience.

4 Real Data Applications

4.1 Data Description

We evaluate our method on three real-world cancer datasets from The Cancer Genome Atlas (TCGA) [37]: COADREAD, STAD, and LGG. The processed multi-omics data and label annotations were obtained from the Broad GDAC Firehose (<https://gdac.broadinstitute.org/>). Each dataset includes matched DNA methylation (X_1), mRNA expression (X_2), and miRNA expression (X_3) data. Only samples with complete data across all three omics types were included in our analysis. The COADREAD dataset combines **CO**lorectal **A**Denocarcinoma (COAD) and **RE**ctal **A**Denocarcinoma (READ) into a binary classification task, with 254 COAD and 78 READ samples. The LGG dataset involves grade classification for low-grade gliomas, with 255 Grade 2 and 269 Grade 3 samples. The STAD dataset targets the classification of **ST**omach **A**Denocarcinoma subtypes, with 205 samples from adenocarcinoma (ADC) and 166 from intestinal adenocarcinoma (IAC). Among the three datasets, COADREAD has the most imbalanced class distribution.

Table 2 summarizes the datasets regarding sample sizes, class distributions, the number of original features, and the number of preprocessed features for each omics type. Data preprocessing includes quality control steps to remove noisy and redundant features, such as filtering out zero-expression signals, low-variance features, and handling multiple comparisons [27]. Each omics dataset was independently normalized to the range [0, 1] using min-max scaling. The preprocessed multi-omics data shared in [27] contains minor inconsistencies in sample sizes across omics modalities. For the COADREAD dataset, meth and mRNA data include 332 samples, while miRNA contains 337 samples. We addressed this discrepancy by removing the five extra miRNA samples to ensure alignment. Similarly, in the STAD dataset, meth and mRNA data comprise 371 samples, whereas miRNA includes 372 samples. Here, we excluded one redundant miRNA sample to maintain consistency.

The histograms in Figure 2 show the distribution of feature values across three omics types (methylation, mRNA, and miRNA) for the COADREAD, LGG, and STAD datasets. The distinct distributional patterns observed across omics types within each dataset highlight each modality's inherent heterogeneity and diverse data characteristics. These differences across the three datasets help evaluate the potential of MOTGNN's generalizability.

Table 2: Data description of three TCGA cancer datasets (COADREAD, LGG, and STAD) regarding sample sizes, class distributions, the number of original features, and the number of preprocessed features for each omics type (methylation, mRNA, and miRNA).

Abbr.	Data Name	Samples	Class Balance (0:1)	Original Features (meth:mRNA:miRNA)	Preprocessed Features (meth:mRNA:miRNA)
COADREAD	Colorectal and Rectal Adenocarcinoma	332	COAD:READ = 254:78	20,113:20,531:420	2,000:2,000:420
LGG	Low-Grade Glioma	524	Grade 2:Grade 3 = 255:269	20,531:20,114:548	2,000:2,000:548
STAD	Stomach Adenocarcinoma	371	ADC:IAC = 205:166	20,101:20,531:507	2,000:2,000:507

Note: meth = DNA methylation, mRNA = gene expression, miRNA = microRNA expression. The processed data were obtained from the Broad GDAC Firehose [27].

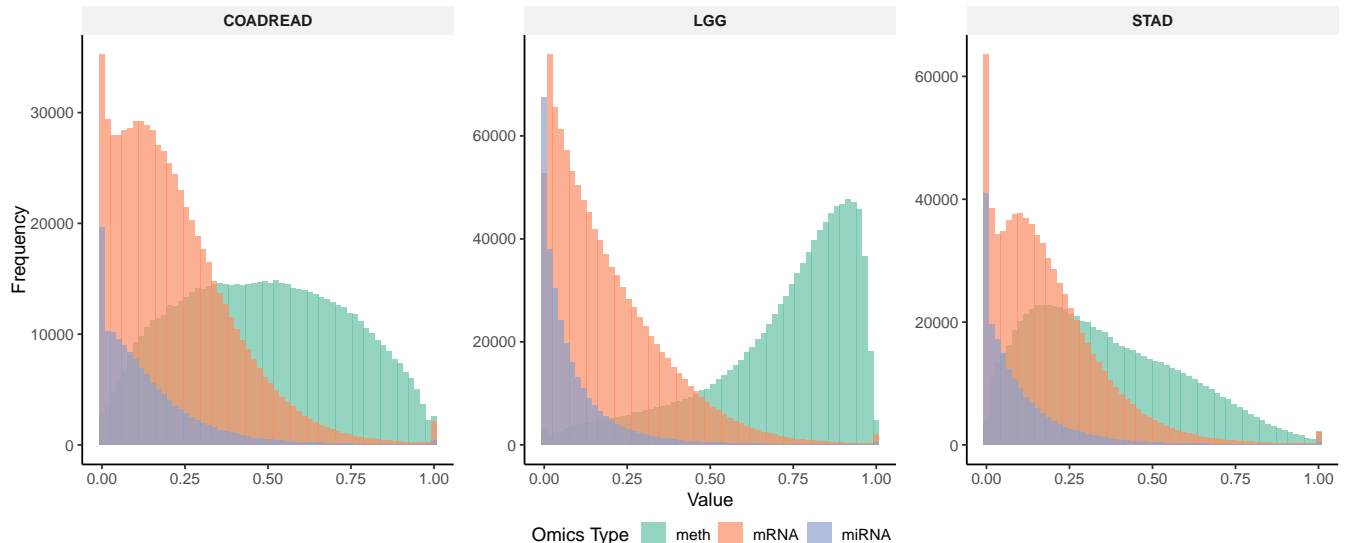


Figure 2: The histogram of methylation, mRNA, and miRNA on preprocessed COADREAD, LGG, and STAD datasets. Each omics dataset was individually scaled to [0, 1]. Different omics types demonstrate distinct distribution patterns.

4.2 Comparison and Evaluation Metrics

We evaluate the performance of our proposed model, MOTGNN, in comparison to several baseline machine learning and deep learning models: XGBoost (XGB) [6], random forest (RF) [4], deep feedforward network (DFN) [11], and graph convolutional network (GCN) [21]. The number of trees for XGBoost and RF is both at the default, which is 100. The number of hidden layers for the DFN and GCN models is two, with several hidden neurons of 64 per layer. All baseline models input the column-wise concatenation of the three preprocessed omics data types (methylation, mRNA, and miRNA). Table 3 summarizes the tuning ranges and selected values (optimal choices in bold). We report three standard evaluation metrics: accuracy, ROC-AUC, and F1-score. Accuracy measures the proportion of correctly classified samples. ROC-AUC (area under the receiver operating characteristic curve) [12] quantifies the model’s ability to distinguish between classes. The F1-score is defined as $F1 = \frac{2 \times \text{precision} \times \text{recall}}{\text{precision} + \text{recall}}$, where precision refers to the positive predictive value, and recall corresponds to sensitivity or true positive rate. As the harmonic mean of precision and recall, the F1-score provides a balanced evaluation, especially in scenarios with imbalanced class

distributions, and mitigates bias from simply predicting the majority class. These metrics comprehensively assess classification performance across different datasets and modeling approaches. We conducted all computations on the Falcon supercomputer [16], requesting four CPUs and 20 GB of memory per job.

5 Results and Discussion

Figure 3 presents the feature dimensions before and after applying XGBoost within the MOTGNN framework. The reduced omics matrices X_1^* , X_2^* , and X_3^* represent the selected feature subsets for DNA methylation, mRNA, and miRNA, respectively. Note that the reduced feature sizes (p_i^*) vary across omics types due to the nature of XGBoost’s feature selection: the final selected set is the union of features used across all M decision trees (see details in Section 3.2). Table 4 highlights the structural properties across MOTGNN’s constructed feature graphs (G_1 - G_3). Figure 4 presents the relative graph importance for the three constructed graphs (G_1 - G_3). The edge-to-node ratios (2.1-2.8) suggest sparse graph structures, with miRNA (G_3) exhibiting the highest edge density (2.35-2.79) but the lowest relative importance (24-29%), indicating limited discriminative value. In COADREAD, mRNA (G_2) dominates (42% importance),

Table 3: Hyperparameter tuning for XGBoost and neural networks components in MOTGNN on COADREAD, LGG, and STAD datasets. The optimal choices are in bold.

Hyperparameter	Tuning Range
<i>XGBoost Parameters</i>	
Number of Trees	100 , 1000
<i>Neural Network Architecture</i>	
Depth (hidden layers)	1, 2, 3
Width (neurons per layer)	32, 64 , 128
Activation Function	ReLU , leakyReLU
<i>Training Parameters</i>	
Learning Rate	0.001, 0.0005, 0.0001
Batch Size	8, 16 , 32
Training Epochs	200, 300, 500
<i>Regularization and Early Stopping</i>	
Dropout Rate	0.2, 0.3, 0.5
L2 Regularization Lambda	0.01
Early Stopping Patience	5, 10
Early Stopping Min Delta	0.001 , 0.005

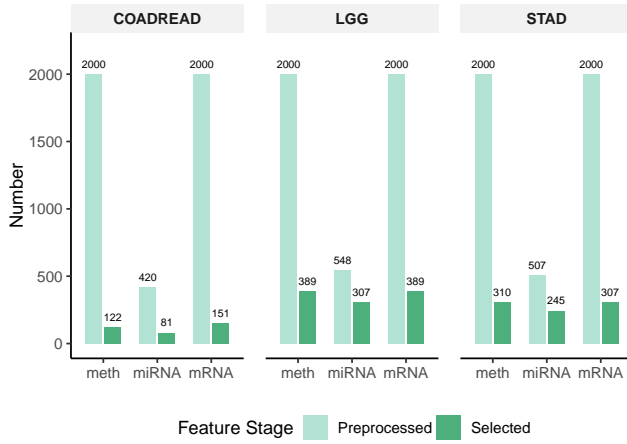


Figure 3: Feature dimensions before and after XGBoost on COADREAD, LGG, and STAD datasets. The bar plots compare the preprocessed feature dimensions (pre-selection) against the reduced dimensions (post-selection).

Table 4: Structural properties of sparse graphs constructed by MOTGNN for COADREAD, LGG, and STAD datasets.

Dataset	Edges ($E_1:E_2:E_3$)	Edge/Node ($m_1:m_2:m_3$)
COADREAD	260:318:190	2.13:2.11:2.35
LGG	880:849:856	2.26:2.18:2.79
STAD	674:646:639	2.17:2.10:2.61

Note: The number of edges includes the self-loops, E_i is the set of edges for Graph G_i , m_i is the edge to node ratio with $m_i = \frac{|E_i|}{|V_i|}$.

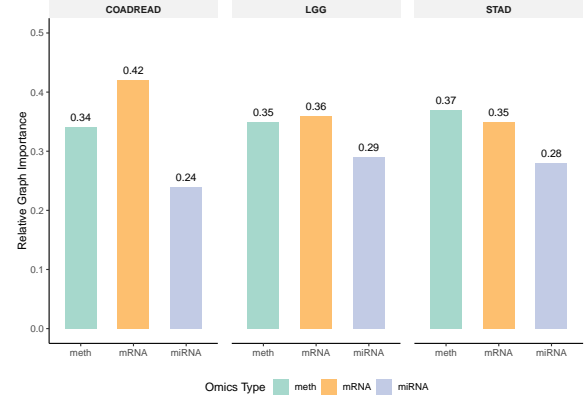


Figure 4: Relative graph importance of different omics types (methylation, mRNA, and miRNA) in MOTGNN's classification performance across COADREAD, LGG, and STAD datasets. Bar heights represent each omics layer's contribution, revealing dataset-specific biological dominance.

Note: G_i = Graphs from reduced features (methylation:mRNA:miRNA), RIG_i = Relative importance of graph G_i in MOTGNN (normalized to sum to 1.0 per dataset).

while methylation (G_1) and mRNA (G_2) contribute equally in LGG and STAD (35-37%). The consistently high methylation importance (34-37%) across datasets underscores its robustness as a biomarker, whereas mRNA's variability reflects tissue-specific expression dynamics. These results demonstrate MOTGNN's ability to prioritize informative omics modalities while maintaining computational efficiency through sparse graph structures, with edge counts remaining tractable for clinical-scale applications.

Table 5 presents classification results averaged over 20 independent train-validation-test splits. Our proposed MOTGNN model consistently outperforms all baselines (XGBoost, RF, DFN, and GCN) across all metrics (Accuracy, ROC-AUC, and F1-score) on all three datasets (COADREAD, LGG, and STAD). In COADREAD, MOTGNN achieves an accuracy of 93.9%, outperforming XGBoost (91.0%), RF (80.1%), DFN (87.3%), and GCN (87.1%). The performance gap is even more evident in F1-score: MOTGNN attains 87.2%, marking a 9.3% absolute improvement over XGBoost (77.9%) and a substantial 53.8% advantage over RF (33.4%). Given COADREAD's imbalanced class distribution (254:78), this improvement highlights MOTGNN's robustness in handling skewed datasets, where traditional models like RF show substantially reduced performance. The ROC-AUC results further validate MOTGNN's stability, with scores exceeding 96.9% for COADREAD and maintaining at least 3% improvements over the best baseline across all datasets. While XGBoost performs competitively in COADREAD (96.4%), its inconsistency becomes apparent when examining results across datasets, dropping to 71.8% for LGG and 63.5% for STAD. DFN shows stronger baseline performance, particularly in STAD (69.1% ROC-AUC), but still falls short of MOTGNN's 71.2%. GCN exhibits moderate performance across datasets and outperforms DFN slightly in LGG and STAD, which suggests some benefit from modeling feature relationships through a graph structure. However, GCN constructs only one graph over concatenated multi-omics features, which may

Table 5: Classification performance comparison on COADREAD, LGG, and STAD datasets across different evaluation metrics (Mean \pm SD [95% CI]). MOTGNN consistently outperforms baseline models across all datasets, highlighting its robustness in integrating multi-omics data (Best results are bolded)

Dataset	Model	Accuracy	ROC-AUC	F1-Score
COADREAD	XGBoost	0.910 \pm 0.034 [0.894, 0.926]	0.964 \pm 0.022 [0.953, 0.975]	0.779 \pm 0.094 [0.735, 0.823]
	RF	0.801 \pm 0.025 [0.789, 0.813]	0.891 \pm 0.038 [0.873, 0.909]	0.334 \pm 0.119 [0.276, 0.392]
	DFN	0.873 \pm 0.043 [0.853, 0.893]	0.926 \pm 0.047 [0.904, 0.948]	0.741 \pm 0.092 [0.696, 0.786]
	GCN	0.871 \pm 0.051 [0.847, 0.895]	0.92 \pm 0.049 [0.897, 0.942]	0.735 \pm 0.107 [0.685, 0.785]
	MOTGNN	0.939 \pm 0.031 [0.925, 0.953]	0.969 \pm 0.023 [0.958, 0.980]	0.872 \pm 0.064 [0.842, 0.902]
LGG	XGBoost	0.663 \pm 0.041 [0.644, 0.682]	0.718 \pm 0.032 [0.703, 0.733]	0.661 \pm 0.041 [0.642, 0.680]
	RF	0.691 \pm 0.051 [0.667, 0.715]	0.764 \pm 0.044 [0.743, 0.785]	0.668 \pm 0.063 [0.638, 0.698]
	DFN	0.691 \pm 0.053 [0.666, 0.716]	0.759 \pm 0.049 [0.736, 0.782]	0.694 \pm 0.052 [0.670, 0.718]
	GCN	0.692 \pm 0.051 [0.668, 0.716]	0.763 \pm 0.049 [0.74, 0.785]	0.693 \pm 0.057 [0.666, 0.719]
	MOTGNN	0.711 \pm 0.038 [0.693, 0.729]	0.777 \pm 0.046 [0.756, 0.798]	0.710 \pm 0.039 [0.692, 0.728]
STAD	XGBoost	0.597 \pm 0.061 [0.569, 0.625]	0.635 \pm 0.070 [0.603, 0.667]	0.542 \pm 0.067 [0.511, 0.573]
	RF	0.628 \pm 0.040 [0.609, 0.647]	0.681 \pm 0.052 [0.657, 0.705]	0.559 \pm 0.053 [0.534, 0.584]
	DFN	0.635 \pm 0.035 [0.619, 0.651]	0.691 \pm 0.049 [0.668, 0.714]	0.595 \pm 0.046 [0.573, 0.617]
	GCN	0.64 \pm 0.047 [0.618, 0.662]	0.694 \pm 0.045 [0.673, 0.715]	0.603 \pm 0.053 [0.578, 0.628]
	MOTGNN	0.664 \pm 0.060 [0.636, 0.692]	0.712 \pm 0.069 [0.680, 0.744]	0.627 \pm 0.063 [0.597, 0.657]

Note: Results are reported as mean \pm standard deviation [95% confidence interval] over 20 runs (n=20). Confidence intervals are calculated using the t-distribution: $CI = \bar{x} \pm t_{0.975,19} \times \frac{SD}{\sqrt{n}}$ where $n = 20$, $t_{0.975,19} = 2.093$. All intervals are symmetric about the mean.

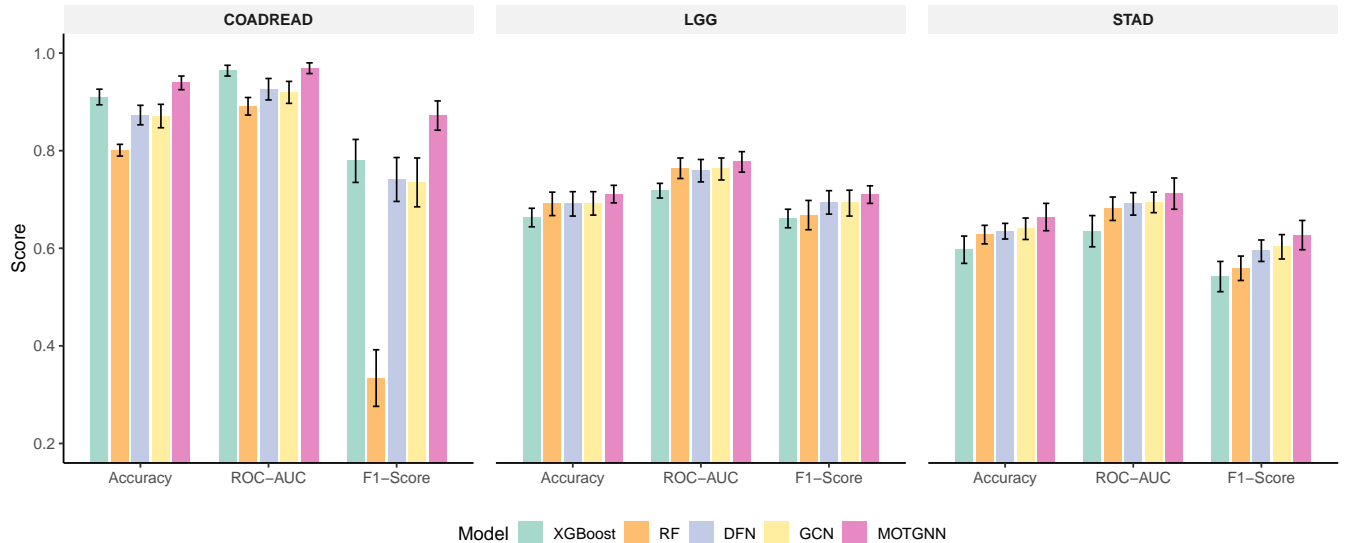


Figure 5: Classification performance comparison for the COADREAD, LGG, and STAD datasets. Bars show mean scores; error bars represent 95% confidence intervals over 20 independent runs.

weaken omics-specific signals and introduce noise from irrelevant cross-omics interactions. In contrast, MOTGNN's modality-specific graph-based architecture provides additional performance gains, particularly under class imbalance, highlighting its suitability for complex biomedical classification tasks.

Figure 5 visually compares model performance across all datasets and evaluation metrics, highlighting MOTGNN's consistent advantage. Although some confidence intervals slightly overlap, MOTGNN consistently achieves higher mean scores. The most significant gaps appear in F1-scores for COADREAD, where MOTGNN (87.2%) far exceeds RF (33.4%), with non-overlapping confidence intervals. The figure also illustrates that, despite XGBoost's strong performance in COADREAD (91% accuracy), its accuracy drops

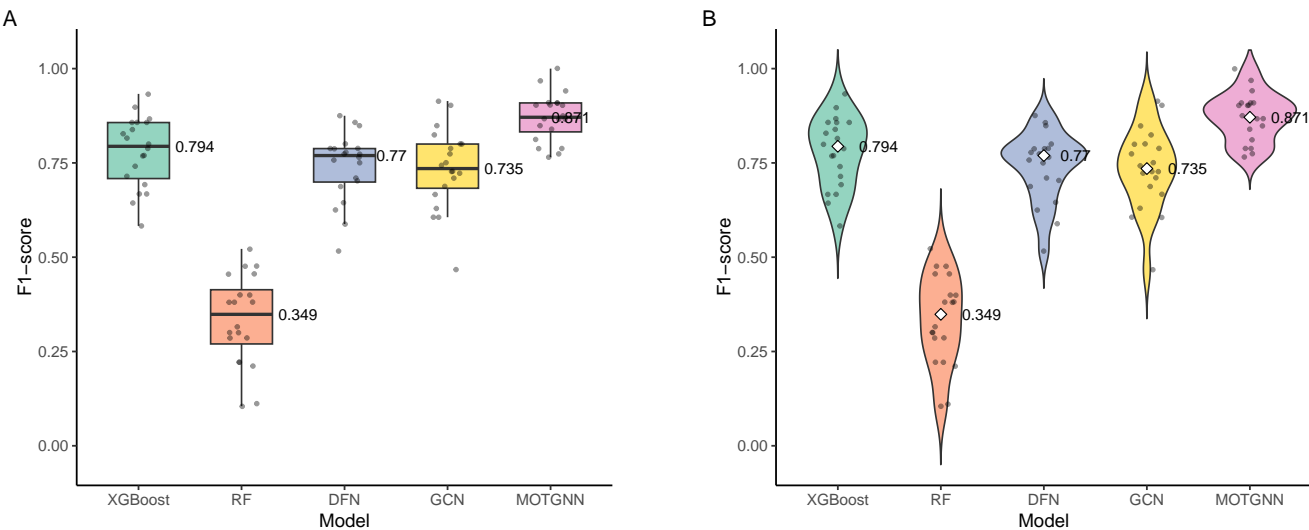


Figure 6: F1-score comparison across 20 runs on the imbalanced COADREAD dataset. (A) Box plots show median (labeled), interquartile range, and outliers. (B) Violin plots show median (labeled) and illustrate score distributions. MOTGNN demonstrates both high performance and low variability.

considerably in LGG and STAD, underscoring its lack of robustness across datasets. Figure 6 highlights model robustness on the imbalanced COADREAD dataset (class ratio 254:78) by comparing F1-scores over 20 independent experiments. MOTGNN achieves the highest median F1-score (0.871), outperforming XGBoost (0.794), DFN (0.771), GCN (0.735), and RF (0.349). The violin plot reveals a tight distribution around MOTGNN's median, indicating low variability. In contrast, XGBoost, DFN, and GCN show wider interquartile ranges, while RF exhibits low performance and high variance. These results underscore MOTGNN's strength in handling class imbalance, a key challenge in biomedical data analysis.

Table 6 presents the top 30 most important biomarkers identified by MOTGNN for the COADREAD dataset (Colorectal Adenocarcinoma and Rectal Adenocarcinoma), illustrating the feature-level interpretability of our framework. COADREAD encompasses colorectal cancer in a broader context and is commonly analyzed jointly, as colon and rectal adenocarcinomas share overlapping molecular signatures and clinical features. This dataset was selected due to its well-characterized molecular landscape and the strong classification performance achieved by our model. The same feature-ranking procedure can also be applied to the other two cancer types: STAD (Stomach Adenocarcinoma) and LGG (Lower Grade Glioma). Among the top-ranked features, Secreted Frizzled-Related Protein 4 (SFRP4) is a well-documented biomarker associated with colorectal cancer [8, 15, 26, 43]. SFRP4 is overexpressed in tumor tissues, and its promoter hypermethylation has been observed as an early event in cancer progression. Functionally, it acts as a modulator of Wnt signaling, thereby influencing cell proliferation and tumor growth. While our current study focuses on computational identification through feature importance scores, biological validation remains an important next step. These selected biomarkers, including SFRP4, serve as potential candidates for further investigation and may

contribute to discovering novel diagnostic or therapeutic strategies for diseases.

Table 6: Top 30 biomarkers identified by MOTGNN for COADREAD by omics type (methylation, mRNA, and miRNA)

Omics type	Biomarkers
meth	LRRC37A2, C9orf70, SNORD98, SFRP4, ELAVL2 HOXD9, HOXC6, DENND2C, MIR519B, DDT4L
mRNA	MUC12 10071, KDELR2 11014, H3F3A 3020 RPL21 6144, AKT1 207, HOXB13 10481 ILVBL 10994, MAEA 10296, PRAC 84366 H3F3C 440093
miRNA	hsa-let-7f-2, hsa-let-7g, hsa-mir-10b, hsa-mir-1201 hsa-mir-1270, hsa-mir-1274b, hsa-mir-191 hsa-mir-206, hsa-mir-30c-2, hsa-mir-425

Note: The COADREAD dataset refers to Colorectal Adenocarcinoma and Rectal Adenocarcinoma (See data details in Table 2). Biomarkers are ranked and selected from three omics types: DNA methylation (meth), gene expression (mRNA), and microRNA expression (miRNA).

Table 7 reveals the computational trade-offs associated with these performance improvements. MOTGNN requires the longest training times, averaging 1.75 minutes for COADREAD and up to 2.39 minutes for LGG, compared to GCN's 0.59-0.94 minutes, DFN's 0.3-0.39 minutes, XGBoost's 0.16-0.25 minutes, and RF's remarkably fast 0.05 minutes per run. However, these computational costs remain practical for real-world applications, especially considering the analysis was conducted using only four CPUs per job. The increased runtime is justified by MOTGNN's superior and stable performance across diverse datasets and metrics.

Table 7: Computation time comparison across models and datasets (in minutes).

Data	Model	Time (min)
COADREAD	XGBoost	0.25
	RF	0.045
	DFN	0.385
	GCN	0.585
LGG	MOTGNN	1.75
	XGBoost	0.195
	RF	0.05
	DFN	0.36
STAD	GCN	0.94
	MOTGNN	2.385
	XGBoost	0.165
	RF	0.05
STAD	DFN	0.3
	GCN	0.805
	MOTGNN	1.45

Note: Each experiment was conducted using only four CPUs without GPU acceleration. The computation time is averaged across 20 independent runs. MOTGNN requires 3-7× longer runtime than XGBoost/RF due to graph construction and hierarchical learning, but remains practical for clinical use (max 2.39 mins)

6 Conclusion

We present MOTGNN, a novel graph neural network framework for multi-omics data integration and disease classification. By leveraging XGBoost for omics-specific supervised graph construction and modality-specific graph neural networks for latent representation learning, MOTGNN effectively captures complex relationships among features that are often overlooked by traditional methods. Applied to real-world cancer datasets, MOTGNN consistently outperforms baseline models across evaluation metrics, demonstrating its strength in integrating heterogeneous omics data and improving predictive performance. In particular, MOTGNN maintains strong robustness under class imbalance, a common challenge in biomedical data analysis. In addition to its predictive power, MOTGNN provides interpretability at both the feature and omics levels. Feature-level importance scores enable the identification of top-ranked biomarkers, which may serve as promising candidates for further biological investigation. Meanwhile, omics-level contributions reveal the relative informativeness of each data modality (e.g., methylation, mRNA, or miRNA), offering valuable insight into their role across different disease types. Future extensions of the MOTGNN framework may include incorporating additional omics modalities, additional cancer types and non-cancer diseases, or adapting the architecture for more complex prediction tasks, such as multi-class classification or survival analysis. Further enhancing interpretability will also be a key direction, especially to better support clinical and biological decision-making.

Data and Code Availability

The harmonized datasets used in our study and the code for our model are available upon request or publication.

Acknowledgments

This work is partially supported by the National Institute of General Medical Sciences of the National Institutes of Health (NIH/NIGMS) under Award P20GM104420. Any findings, comments, and conclusions expressed in this paper do not reflect the views of NIH.

References

- [1] Martín Abadi, Paul Barham, Jianmin Chen, Zhifeng Chen, Andy Davis, Jeffrey Dean, Matthieu Devin, Sanjay Ghemawat, Geoffrey Irving, Michael Isard, et al. 2016. {TensorFlow}: A System for {Large-Scale} Machine Learning. In *12th USENIX symposium on operating systems design and implementation (OSDI 16)*. 265–283.
- [2] Hazem Ayman, Madonna Bassem, Malak Madkour, Mariam Fawzi, Nada Amr, Youmna Yousry, Ziad Elgayar, and Ashraf Abdelraouf. 2023. A Review of Multi-omics and Machine Learning: Advancements and Applications in Cancer Research. In *2023 International Mobile, Intelligent, and Ubiquitous Computing Conference (MIUCC)*. IEEE, 1–8.
- [3] Jenna L Ballard, Zexuan Wang, Wenrui Li, Li Shen, and Qi Long. 2024. Deep learning-based approaches for multi-omics data integration and analysis. *BioData Mining* 17, 1 (2024), 38.
- [4] Leo Breiman. 2001. Random forests. *Machine learning* 45, 1 (2001), 5–32.
- [5] Michael M Bronstein, Joan Bruna, Yann LeCun, Arthur Szlam, and Pierre Vandergheynst. 2017. Geometric deep learning: going beyond euclidean data. *IEEE Signal Processing Magazine* 34, 4 (2017), 18–42.
- [6] Tianqi Chen and Carlos Guestrin. 2016. Xgboost: A scalable tree boosting system. In *Proceedings of the 22nd ACM SIGKDD international conference on knowledge discovery and data mining*. 785–794.
- [7] Zhiqian Chen, Fanglan Chen, Lei Zhang, Taoran Ji, Kaiqun Fu, Liang Zhao, Feng Chen, Lingfei Wu, Charu Aggarwal, and Chang-Tien Lu. 2023. Bridging the gap between spatial and spectral domains: A unified framework for graph neural networks. *Comput. Surveys* 56, 5 (2023), 1–42.
- [8] Bernd Frank, Michael Hoffmeister, Norman Klopp, Thomas Illig, Jenny Chang-Claude, and Hermann Brenner. 2010. Single nucleotide polymorphisms in Wnt signaling and cell death pathway genes and susceptibility to colorectal cancer. *Carcinogenesis* 31, 8 (2010), 1381–1386.
- [9] Jerome H Friedman. 2002. Stochastic gradient boosting. *Computational statistics & data analysis* 38, 4 (2002), 367–378.
- [10] Justin Gilmer, Samuel S Schoenholz, Patrick F Riley, Oriol Vinyals, and George E Dahl. 2017. Neural message passing for quantum chemistry. In *International conference on machine learning*. PMLR, 1263–1272.
- [11] Ian Goodfellow, Yoshua Bengio, and Aaron Courville. 2016. *Deep learning*. MIT press.
- [12] David Marvin Green, John A Swets, et al. 1966. *Signal detection theory and psychophysics*. Vol. 1. Wiley New York.
- [13] Will Hamilton, Zhitao Ying, and Jure Leskovec. 2017. Inductive representation learning on large graphs. *Advances in neural information processing systems* 30 (2017).
- [14] Leroy Hood and Lee Rowen. 2013. The Human Genome Project: big science transforms biology and medicine. *Genome medicine* 5 (2013), 1–8.
- [15] Dan Huang, Bi Yu, Yun Deng, Weiqi Sheng, Zhilei Peng, Wenxin Qin, and Xiang Du. 2010. SFRP4 was overexpressed in colorectal carcinoma. *Journal of cancer research and clinical oncology* 136 (2010), 395–401.
- [16] Idaho C3+3 Collaboration. 2022. Falcon: High Performance Supercomputer. <https://doi.org/10.7923/falcon.id>. Accessed: 2025-06-05.
- [17] Wei Jiang, Weicai Ye, Xiaoming Tan, and Yun-Juan Bao. 2025. Network-based multi-omics integrative analysis methods in drug discovery: a systematic review. *BioData Mining* 18, 1 (2025), 27.
- [18] Ruth Johnson, Michelle M Li, Ayush Noori, Owen Queen, and Marinka Zitnik. 2024. Graph artificial intelligence in medicine. *Annual review of biomedical data science* 7, 2024 (2024), 345–368.
- [19] Ziynet Nesibe Kesimoglu and Serdar Bozdag. 2023. SUPREME: multiomics data integration using graph convolutional networks. *NAR Genomics and Bioinformatics* 5, 2 (2023), lqad063.
- [20] Diederik P Kingma and Jimmy Ba. 2014. Adam: A method for stochastic optimization. *arXiv preprint arXiv:1412.6980* (2014).
- [21] Thomas N Kipf and Max Welling. 2017. Semi-Supervised Classification with Graph Convolutional Networks. In *International Conference on Learning Representations*.
- [22] Yunchuan Kong and Tianwei Yu. 2018. A graph-embedded deep feedforward network for disease outcome classification and feature selection using gene expression data. *Bioinformatics* 34, 21 (2018), 3727–3737.
- [23] Yunchuan Kong and Tianwei Yu. 2020. forgeNet: a graph deep neural network model using tree-based ensemble classifiers for feature graph construction. *Bioinformatics* 36, 11 (2020), 3507–3515.

[24] Yann Lecun, Yoshua Bengio, and Geoffrey Hinton. 2015. Deep learning. *Nature* 521, 7553 (2015), 436–444. doi:10.1038/nature14539

[25] Xiao Li, Jie Ma, Ling Leng, Mingfei Han, Mansheng Li, Fuchu He, and Yunping Zhu. 2022. MoGCN: a multi-omics integration method based on graph convolutional network for cancer subtype analysis. *Frontiers in Genetics* 13 (2022), 806842.

[26] Yuting Liu, Jun Yu, Yang Xie, Mengying Li, Feng Wang, Jing Zhang, and Jian Qi. 2020. EZH2 regulates sFRP4 expression without affecting the methylation of sFRP4 promoter DNA in colorectal cancer cell lines. *Experimental and therapeutic medicine* 20, 5 (2020), 33.

[27] Yuxing Lu, Rui Peng, Lingkai Dong, Kun Xia, Renjie Wu, Shuai Xu, and Jinzhao Wang. 2023. Multiomics dynamic learning enables personalized diagnosis and prognosis for pancreatic and cancer subtypes. *Briefings in Bioinformatics* 24, 6 (11 2023). doi:10.1093/bib/bbad378

[28] Vinod Nair and Geoffrey E Hinton. 2010. Rectified linear units improve restricted boltzmann machines. In *Icm*.

[29] Julian D Olden and Donald A Jackson. 2002. Illuminating the “black box”: a randomization approach for understanding variable contributions in artificial neural networks. *Ecological modelling* 154, 1-2 (2002), 135–150.

[30] Showmick Guha Paul, Arpa Saha, Md Zahid Hasan, Shek Rashed Haider Noori, and Ahmed Moustafa. 2024. A systematic review of graph neural network in healthcare-based applications: Recent advances, trends, and future directions. *IEEE Access* 12 (2024), 15145–15170.

[31] Velicković Petar, Cucurull Guillem, Casanova Arantxa, Romero Adriana, Lio Pietro, and B Yoshua. 2018. Graph attention networks. In *International conference on learning representations*, Vol. 8.

[32] Indhupriya Subramanian, Srikant Verma, Shiva Kumar, Abhay Jere, and Krishnanpal Anamika. 2020. Multi-omics data integration, interpretation, and its application. *Bioinformatics and biology insights* 14 (2020), 117932219899051.

[33] Raihanul Bari Tanvir, Md Mezbahul Islam, Masrur Sobhan, Dongsheng Luo, and Ananda Mohan Mondal. 2024. MOGAT: a multi-omics integration framework using graph attention networks for cancer subtype prediction. *International Journal of Molecular Sciences* 25, 5 (2024), 2788.

[34] Nektarios A Valous, Ferdinand Popp, Inka Zörnig, Dirk Jäger, and Pornpimol Charoentong. 2024. Graph machine learning for integrated multi-omics analysis. *British journal of cancer* 131, 2 (2024), 205–211.

[35] Tongxin Wang, Wei Shao, Zhi Huang, Haixu Tang, Jie Zhang, Zhengming Ding, and Kun Huang. 2021. MOGONET integrates multi-omics data using graph convolutional networks allowing patient classification and biomarker identification. *Nature communications* 12, 1 (2021), 3445.

[36] Asim Waqas, Aakash Tripathi, Ravi P Ramachandran, Paul A Stewart, and Ghulam Rasool. 2024. Multimodal data integration for oncology in the era of deep neural networks: a review. *Frontiers in Artificial Intelligence* 7 (2024), 1408843.

[37] John N Weinstein, Eric A Collisson, Gordon B Mills, Kenna R Shaw, Brad A Ozenberger, Kyle Ellrott, Ilya Shmulevich, Chris Sander, and Joshua M Stuart. 2013. The cancer genome atlas pan-cancer analysis project. *Nature genetics* 45, 10 (2013), 1113–1120.

[38] Jiecheng Wu, Zhaoliang Chen, Shunxin Xiao, Gengcheng Liu, Wenjie Wu, and Shiping Wang. 2024. DeepMoIC: multi-omics data integration via deep graph convolutional networks for cancer subtype classification. *BMC genomics* 25, 1 (2024), 1–13.

[39] Zonghan Wu, Shirui Pan, Fengwen Chen, Guodong Long, Chengqi Zhang, and Philip S Yu. 2020. A comprehensive survey on graph neural networks. *IEEE transactions on neural networks and learning systems* 32, 1 (2020), 4–24.

[40] Keyulu Xu, Weihua Hu, Jure Leskovec, and Stefanie Jegelka. 2019. How powerful are graph neural networks? In *International Conference on Learning Representations*.

[41] Hu Yang, Zhong Zhuang, and Wei Pan. 2021. A graph convolutional neural network for gene expression data analysis with multiple gene networks. *Statistics in Medicine* 40, 25 (2021), 5547–5564.

[42] Xiaohui Yao, Xiaohan Jiang, Haoran Luo, Hong Liang, Xiufen Ye, Yanhui Wei, and Shan Cong. 2024. Mocat: multi-omics integration with auxiliary classifiers enhanced autoencoder. *BioData Mining* 17, 1 (2024), 9.

[43] Pengcheng Yu, Weiyang He, Yanqiang Zhang, Can Hu, Yue Wu, Yi Wang, Zhehan Bao, Yuhang Xia, Ruolan Zhang, Mengxuan Cao, et al. 2022. Sfrp4 is a potential biomarker for the prognosis and immunotherapy for gastric cancer. *Journal of Oncology* 2022, 1 (2022), 8829649.

[44] Shaza B Zaghloul and Omneya Attallah. 2022. A review of deep learning methods for multi-omics integration in precision medicine. In *2022 IEEE International Conference on Bioinformatics and Biomedicine (BIBM)*. IEEE, 2208–2215.

[45] Xiao-Meng Zhang, Li Liang, Lin Liu, and Ming-Jing Tang. 2021. Graph neural networks and their current applications in bioinformatics. *Frontiers in genetics* 12 (2021), 690049.

[46] Ziwei Zhang, Peng Cui, and Wenwu Zhu. 2020. Deep learning on graphs: A survey. *IEEE Transactions on Knowledge and Data Engineering* 34, 1 (2020), 249–270.

[47] Chen Zhao, Anqi Liu, Xiao Zhang, Xuewei Cao, Zhengming Ding, Qiuying Sha, Hui Shen, Hong Wen Deng, and Weihua Zhou. 2024. CLCLSA: Cross-omics linked embedding with contrastive learning and self attention for integration with incomplete multi-omics data. *Computers in Biology and Medicine* 170 (3 2024). doi:10.1016/j.combiomed.2024.108058

[48] Yating Zhong, Yuzhong Peng, Yanmei Lin, Dingjia Chen, Hao Zhang, Wen Zheng, Yuanyuan Chen, and Changliang Wu. 2023. MODILM: towards better complex diseases classification using a novel multi-omics data integration learning model. *BMC Medical Informatics and Decision Making* 23, 1 (2023), 82.

[49] Zhiqiang Zhong, Anastasia Barkova, and Davide Mottin. 2025. Knowledge-augmented Graph Machine Learning for Drug Discovery: A Survey. *ACM Comput. Surv.* (2025). <https://doi.org/10.1145/3744237>

[50] Jie Zhou, Ganqu Cui, Shengding Hu, Zhengyan Zhang, Cheng Yang, Zhiyuan Liu, Lifeng Wang, Changcheng Li, and Maosong Sun. 2020. Graph neural networks: A review of methods and applications. *AI open* 1 (2020), 57–81.